The Morphometry of Impact Craters on Bennu

R.T. Daly, E. Bierhaus, Olivier Barnouin, Mike Daly, J. Seabrook, James Roberts, Carolyn Ernst, Mark E. Perry, Nair H, R.C. Esperitu, et al.

HAL Id: hal-03085217
https://hal.science/hal-03085217

Submitted on 21 Dec 2020

Geophysical Research Letters

Key Points:
- The depth-to-diameter ratio (d/D) of asteroid Bennu's craters >10 m in diameter ranges from 0.02 to 0.19 with a mean of 0.10 ± 0.03
- Small craters show the greatest diversity in d/D, whereas larger craters (>80 m) span a narrower range in d/D and tend to be shallower
- For craters >80 m, increases in target strength with depth, combined with target curvature, likely contribute to smaller d/D

Supporting Information:
- Supporting Information S1
- Table S1

Correspondence to:
R. T. Daly,
terik.daly@jhuapl.edu

The Morphometry of Impact Craters on Bennu

R. T. Daly[1] , E. B. Bierhaus[2] , O. S. Barnouin[1] , M. G. Daly[3] , J. A. Seabrook[3] , J. H. Roberts[1] , C. M. Ernst[1] , M. E. Perry[1] , H. Nair[1] , R. C. Espiritu[1] , E. E. Palmer[4] , R. W. Gaskell[4] , J. R. Weirich[4] , H. C. M. Susorney[5] , C. L. Johnson[5,6] , K. J. Walsh[7] , M. C. Nolan[8] , E. R. Jawin[9] , P. Michel[10] , D. Trang[11] , and D. S. Lauretta[8]

[1]Johns Hopkins University Applied Physics Laboratory, Laurel, MD, USA, [2]Lockheed Martin Space, Littleton, CO, USA, [3]Centre for Research in Earth and Space Science, York University, Toronto, Ontario, Canada, [4]Planetary Science Institute, Tucson, AZ, USA, [5]School of Earth Sciences, University of Bristol, Bristol, UK, [6]Department of Earth, Ocean and Atmospheric Sciences, University of British Columbia, Vancouver, British Columbia, Canada, [7]Southwest Research Institute, Boulder, CO, USA, [8]Lunar and Planetary Laboratory, University of Arizona, Tucson, AZ, USA, [9]Smithsonian Institution National Museum of Natural History, Washington, DC, USA, [10]Observatoire de la Côte d'Azur, CNRS, Laboratoire Lagrange, Université Côte d'Azur, Nice, France, [11]Hawai'i Institute of Geophysics and Planetology, University of Hawai'i at Mānoa, Honolulu, HI, USA

Abstract Bennu is an ~500-m-diameter rubble-pile asteroid that is the target of detailed study by the Origins, Spectral Interpretation, Resource Identification, and Security–Regolith Explorer (OSIRIS-REx) mission. Here we use data from the OSIRIS-REx Laser Altimeter to assess depth-to-diameter ratios (d/D) of 108 impact craters larger than 10 m in diameter. The d/D of craters on Bennu ranges from 0.02 to 0.19. The mean is 0.10 ± 0.03. The smallest craters show the broadest range in d/D, consistent with d/D measurements on other asteroids. A few craters have central mounds, which is interpreted as evidence that a more competent substrate lies a few meters beneath them. The range of d/D narrows as crater size increases, with craters larger than 80 m tending toward smaller d/D. At large scales, increases in target strength with depth, combined with target curvature, may affect crater morphometry.

Plain Language Summary Between 2018 and 2020, National Aeronautics and Space Administration (NASA)'s Origins, Spectral Interpretation, Resource Identification, and Security–Regolith Explorer (OSIRIS-REx) spacecraft orbited a small asteroid called Bennu in preparation to collect a sample for return to Earth. Bennu is a "rubble-pile" asteroid, meaning an aggregate of rock fragments that have coalesced together in space. OSIRIS-REx observations showed that Bennu has many craters on its surface, which formed when other, smaller objects collided with it in the past. Crater depths and widths (diameters), in addition to relating to the size and speed of the impacting object, also reflect the physical characteristics of the impacted surface. Accordingly, we measured the depths and diameters of many of Bennu's craters to better understand the surface and interior properties of this rubble-pile asteroid and how it compares to other asteroids. The smaller craters on Bennu have a variety of depths, even among similarly sized craters. The largest are so wide that they appear to be affected by the curvature of Bennu's surface and by the presence of stronger material at depth. We observe mounds inside some of the smaller craters, supporting the idea that a more competent substrate underlies the surface material.

1. Introduction

The near-Earth asteroid (101955) Bennu is the target of National Aeronautics and Space Administration (NASA)'s Origins, Spectral Interpretation, Resource Identification, and Security–Regolith Explorer (OSIRIS-REx) mission (Lauretta et al., 2015, 2017). Bennu is a small, low-albedo, B-type asteroid (Hergenrother et al., 2013) with an average radius of 244 m (Barnouin, Daly, Palmer, et al., 2019). OSIRIS-REx observations confirmed that Bennu is a rubble-pile asteroid (Barnouin, Daly, Palmer, et al., 2019; Lauretta et al., 2019; Walsh et al., 2019) with widespread hydrated minerals across its surface (Hamilton et al., 2019).

OSIRIS-REx's initial survey revealed multiple impact craters on Bennu's surface (Walsh et al., 2019). Further searches with higher-resolution data sets found hundreds of candidate impact craters (Bierhaus, Barnouin, McCoy, et al., 2019; Bierhaus, Barnouin, Walsh, et al., 2019). Impact craters provide clues to the physical properties and age of Bennu's surface, as well as the processes that have shaped Bennu into its present

form. They also yield insights into cratering mechanics. Cratering on Bennu occurs in a challenging-to-understand regime that pushes the frontiers of our understanding of impact mechanics: gravity is very small (Lauretta et al., 2019; Scheeres et al., 2019); target strength is low (Ballouz et al., 2020; Lauretta et al., 2019; Scheeres et al., 2019) but poorly known and could vary with depth (Barnouin, Daly, Palmer, et al., 2019); target porosity is high (Barnouin, Daly, Palmer, et al., 2019; Scheeres et al., 2019); and the target surface is coarse grained and boulder rich (Barnouin, Daly, Palmer, et al., 2019; DellaGiustina et al., 2019; Lauretta et al., 2019; Walsh et al., 2019).

Craters are distributed across the surface of Bennu (Bierhaus, Barnouin, McCoy, et al., 2019; Bierhaus, Barnouin, Walsh, et al., 2019), with several large, distinct craters located on Bennu's equatorial ridge (Walsh et al., 2019). The most distinct impact craters are circular features with raised rims and depressed floors and, in some cases, textural differences between the interior and exterior of the crater (Walsh et al., 2019). Less distinct craters have muted or absent raised rims and shallow interiors (Walsh et al., 2019). Craters range in size from ~160 m (Walsh et al., 2019) to as small as several centimeters. These smallest craters were discovered on the faces of boulders (Ballouz et al., 2020). Impact craters have a variety of interior morphologies, which have been attributed to local variations in the preimpact boulder population and the size of the craters relative to the boulders (Bierhaus et al., 2020).

Impact crater depth-to-diameter relationships (d/D) have been studied on several asteroids, including Vesta, Lutetia, Steins, Ida, Mathilde, Eros, Gaspra, and Itokawa; see Marchi et al. (2015) for a review. Preliminary results for a few large craters on asteroid (162173) Ryugu have also been reported (Noguchi et al., 2021). Here, we assess d/D on Bennu to characterize its impact craters and assess the implications for its surface and interior.

2. Materials and Methods

2.1. Impact Crater Selection

Impact craters on Bennu were found by examining images acquired by the OSIRIS-REx Camera Suite (OCAMS) (Golish et al., 2020; Rizk et al., 2018) during the Approach, Preliminary Survey, and Detailed Survey phases of the OSIRIS-REx mission (Lauretta et al., 2017). OCAMS imaged Bennu globally at a range of illumination and viewing geometries (DellaGiustina et al., 2019), and multiple OSIRIS-REx team members searched the images for craters (Walsh et al., 2019). Identified craters were combined into a global crater database (Bierhaus, Barnouin, Walsh, et al., 2019; Bierhaus, Barnouin, McCoy, et al., 2019; Bierhaus et al., 2020; Walsh et al., 2019). Craters analyzed here were selected from the October 2019 version of the crater database, which contained 135 crater candidates larger than ~10 m in diameter. This size cutoff was chosen based on the horizontal ground-sample distance of topographic data products developed in the first few months of Bennu arrival and to keep the total number of craters manageable for this initial study. Of these, 108 craters were included in the d/D analyses. The remaining candidates were excluded because they lacked a topographic expression (i.e., no depressed interior with a discernable rim around at least part of the crater circumference), substantially overlapped another crater, or had a large boulder in their center.

2.2. Depth and Diameter Measurements

We measured impact crater depths and diameters using digital terrain models (DTMs) derived from data collected by the OSIRIS-REx Laser Altimeter (OLA) (Barnouin et al., 2020; Daly et al., 2017). Supporting information Text S1 details the OLA data set and DTM creation.

From each crater DTM, we extracted topographic elevation profiles at eight evenly spaced azimuths by means of a semiautomated IDL code. Rim-to-rim diameter and rim-to-floor depth were determined along each profile. The user specified the deepest point to be used (based on examination of images and the DTMs) so that the depths were not biased by features such as crevices between boulders. Using multiple topographic profiles is consistent with recommended best practices for d/D studies (Robbins et al., 2018).

We report crater depths with respect to elevation (i.e., relative to a reference geopotential, Figure S1). This approach is needed to evaluate surface processes (e.g., slope failure) that may affect craters and to measure the depths of craters formed on slopes. On larger bodies (e.g., the Moon, Mercury, and Mars), d/D measurements are implicitly made relative to a geoid.

Individual profile(s) of a crater were excluded in cases when a profile passed through an anomalous structure on the rim (e.g., very large boulder and adjacent crater), when a rim point could not be discerned (e.g., on the downslope side of a crater wall), or, for craters >100 m in diameter, when body curvature made the center of the crater higher than the rims for a specific profile (e.g., N-S profiles of large equatorial craters). The remaining profiles were averaged to compute rim-to-rim diameter, rim-to-floor depth, and thereby d/D. The uncertainties reported here represent the standard deviation of the depths and diameters of all the profiles deemed useable for a given crater. The automated IDL code generated eight profiles for each crater; after human evaluation of the profiles, a crater could have as many as eight to as few as two profiles.

In addition to the standard deviation, the number of profiles used for a crater can be a metric for how much weight one can give an individual crater when interpreting the data. Craters quantified using many profiles were easier to analyze than craters for which only a few profiles could be used. Small numbers of profiles can lead to small standard deviations, whereas the small number of profiles indicates the crater was challenging to evaluate. The supporting information table that accompanies this manuscript lists the number of profiles used for each crater.

3. Results

Figure 1 shows six representative craters that range in diameter from 11.5 ± 0.9 to 161.0 ± 5.7 m, as shown in radiometrically calibrated images taken by OCAMS, as well as the DTMs colored by elevation.

Figure 2 shows elevation profiles for these same craters. Some of the craters (e.g., Figure 2b) are symmetric, while many (e.g., Figures 2a, 2c, 3d, and 2e) are not. Some formed on regional slopes (e.g., Figures 2a and 2c–2e). Craters formed on slopes are asymmetric in the slope direction, with a muted wall on the downslope side.

Figure 3 shows the relationship between impact crater depth and diameter on Bennu for the 108 craters larger than 10 m that we included in our data set. Values of d/D range from 0.02 to 0.19, with a mean value of 0.10 ± 0.03. The distribution is unimodal. The range of d/D is a function of crater size, with the largest diversity at small sizes, and a narrowing range of d/D—tending toward smaller values—as crater size increases (Figure 3b). For craters larger than 80 m, d/D ranges only from 0.02 to 0.09; the average is 0.06. These craters are large relative to the total size of Bennu: 80 m is ~16% of Bennu's diameter.

Three craters have mounds near their centers (Figure S3). The mounds do not appear to be partially exposed or partially buried boulders. The diameters of mound craters range from ~15 to ~22 m, and the mounds are apparent in many of the topographic profiles (Figure S4). These craters are geographically dispersed. Two of the three are located on flat areas, while the crater in Figure S3A is superposed on an ~14° regional slope. The d/D of these three craters is unremarkable compared to the rest of the population (for the purposes of calculating crater depth, the deepest point was chosen to be off to one side of the mound). In all three cases, the mound diameter is ~0.3 times the diameter of the crater (Table S3). Two other craters may have mounds, but the data are ambiguous.

4. Discussion

4.1. Comparisons to d/D on Other Asteroids

Asteroids Ryugu and (253) Mathilde are likely similar to Bennu in composition based on their C-complex taxonomic type, and all three are highly porous (Veverka, 1997; Watanabe et al., 2019), but their gravitational accelerations differ substantially. Hence, Ryugu and Mathilde provide useful points of reference. Two studies have reported d/D for impact craters on Ryugu. Sugita et al. (2019) reported that the d/D of a few impact craters on Ryugu larger than 20 m in diameter ranged from 0.14 to 0.2. Noguchi et al. (2021) report that the mean d/D of all 77 craters on Ryugu is 0.09 ± 0.02, with a range of 0.03–0.15. Noguchi et al. (2021) attribute the differences between the two studies to differences in how the measurements were made (see Figure S1 in Noguchi et al., 2021). Both studies used a different approach than the one used here. The Sugita et al. (2019) results suggest that craters on Ryugu are deeper than craters on Bennu, whereas the Noguchi et al. (2021) results are similar to the results for Bennu. Thomas et al. (1999) reported that the d/D of four craters on Mathilde ranged from 0.12 to 0.25, with uncertainties of at least 25%, which suggests that craters on Mathilde tend to be deeper than those on Bennu or Ryugu. We speculate that the orders-
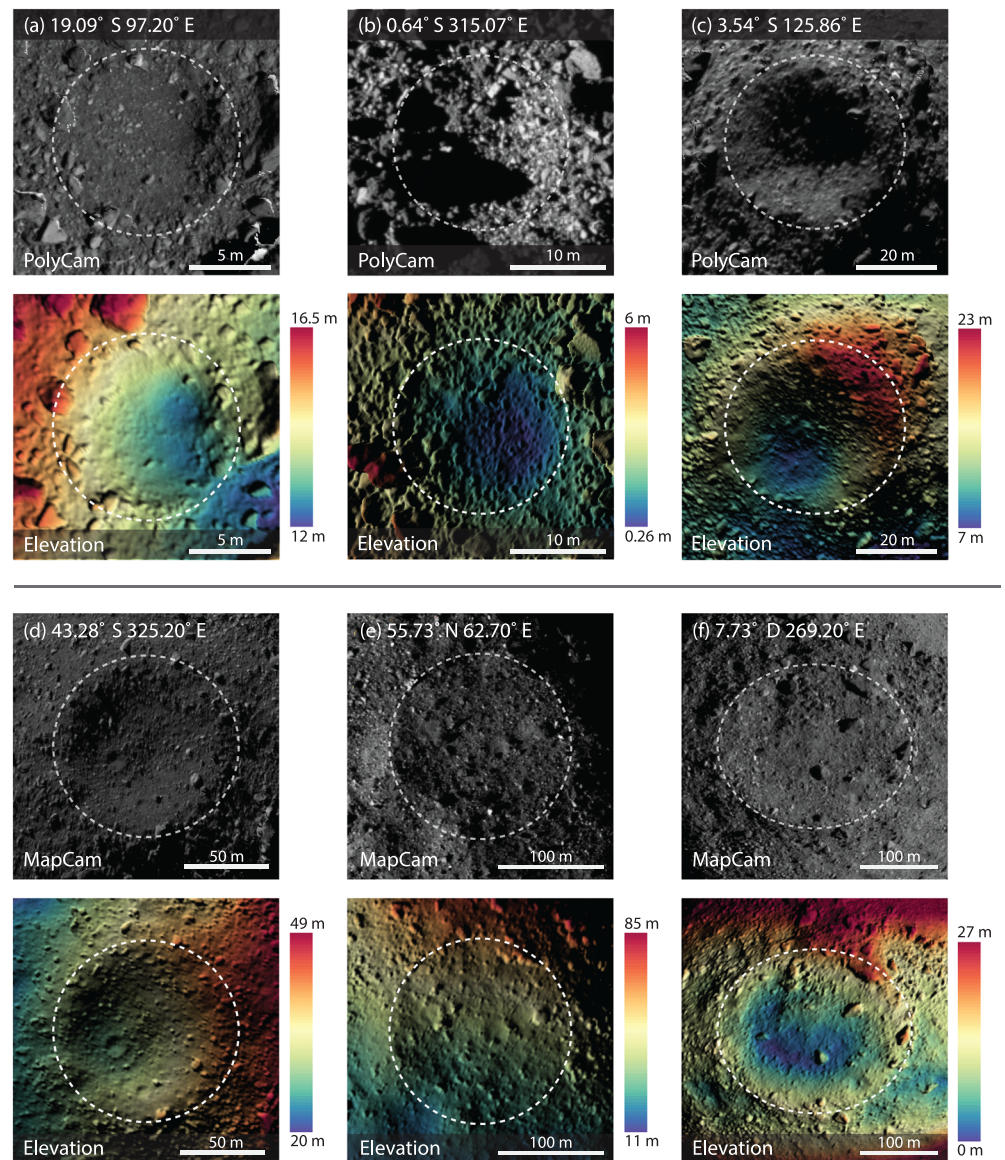
Figure 1. Images and rendered DTMs of representative impact craters on Bennu. The top row shows image(s) of craters acquired by the OCAMS PolyCam or MapCam instrument, overlaid on the DTMs. The bottom row shows renderings of DTM elevation, and the DTMs are illuminated to match the solar illumination conditions in the image. Table S2 gives the image names and other information about the images shown here.

of-magnitude stronger gravitational acceleration on Mathilde may contribute to these differences, though the limited data set for Mathilde and differences in how the measurements were made must be kept in mind.

Of the asteroids with spectral types (and therefore compositions) that differ from Bennu's, d/D is most similar to that on Itokawa, where d/D ranges from 0.01 to 0.15 (Hirata et al., 2009). The similar d/D on Itokawa and Bennu, despite their differences in composition and bulk density, may indicate that intergranular porosity and granular dynamics influence d/D on rubble-pile asteroids more than compositional differences.

4.2. Potential for Crater Degradation via Mass Movement

Variation in degradation state likely contributes to the broad range of d/D on Bennu. On Vesta and Lutetia, differences in degradation state have been interpreted as the key drivers of d/D diversity at small scales (Marchi et al., 2015; Vincent et al., 2012, 2014). Small craters on Bennu also show the most variation in
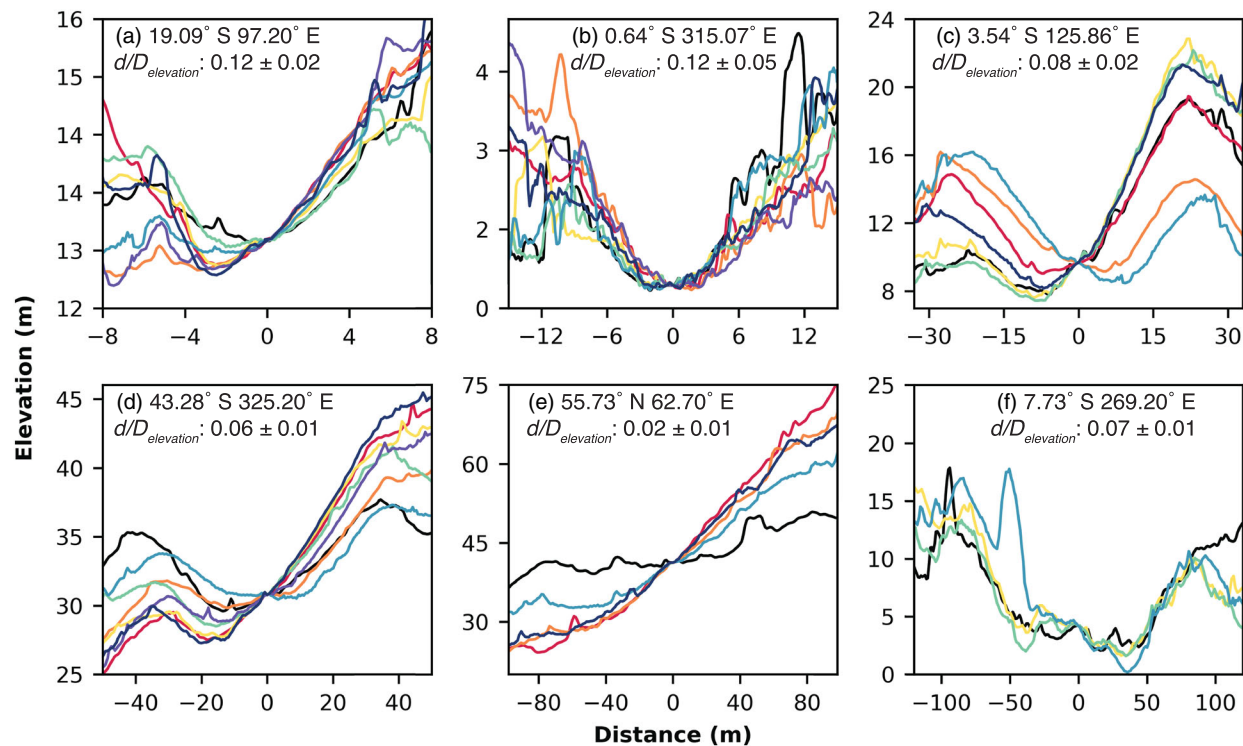
Figure 2. Topographic profiles of six representative impact craters shown in Figure 1. Each color shows a profile taken at a different azimuth; Figure S2 shows profile locations and directions.

d/D. Deeper craters of a given size are typically interpreted as fresher (e.g., Barnouin-Jha et al., 2001; Carr et al., 1994; Cheng et al., 2002; Sullivan et al., 1996; Vincent et al., 2012, 2014).

The extent of degradation should be a function of both crater age (older craters should be more degraded than younger ones) and the level of geologic activity in an area (craters in regions prone to resurfacing should be more degraded than similarly aged craters in less active regions). Based on maps of mass movement events on Bennu, Jawin et al. (2020) inferred that between ~5 and 10 m of material could have been removed from the lower midlatitudes and transported equatorward, potentially contributing to crater infilling and erasure along the way.

We can assess the potential importance of mass-movement-driven resurfacing on impact crater *d/D* globally by looking for correlations between *d/D* and areas prone to mass movement. On Bennu, the steepest slopes are currently located between 30° and 70° latitude in both the northern and southern hemispheres, and these regions are the most prone to mass movement (Barnouin, Daly, Palmer, et al., 2019). The primary direction of mass movement on Bennu is from the polar and midlatitude regions toward the equatorial region, here defined as ±20° latitude (Jawin et al., 2020). The equatorial ridge is the ultimate sink for downslope movement of material (Daly et al., 2020). If mass movement were a dominant factor in *d/D* variations, *d/D* would decrease from the poles toward the equator.

For a subset of 39 craters that are likely fresh (deeper than average *d/D)* and susceptible to infilling by mass movement, we find some evidence in the southern hemisphere of decreasing *d/D* between ~60°S and 30°S, but the trend does not unambiguously continue to the equator (Figure S5). This trend is not seen in the northern hemisphere, a difference that may be related to the larger-scale contrasts in the shape and topography, and perhaps material properties, of the northern and southern hemispheres reported by Daly et al. (2020). Mass movement alone cannot explain the variations in *d/D* on Bennu.

4.3. Other Factors That Likely Contribute to *d/D* Variations

In addition to crater degradation, variations in target properties contribute to *d/D* diversity. Properties such as porosity and strength affect impactor penetration and coupling and thus *d/D* (Schultz, 1988). Variations in
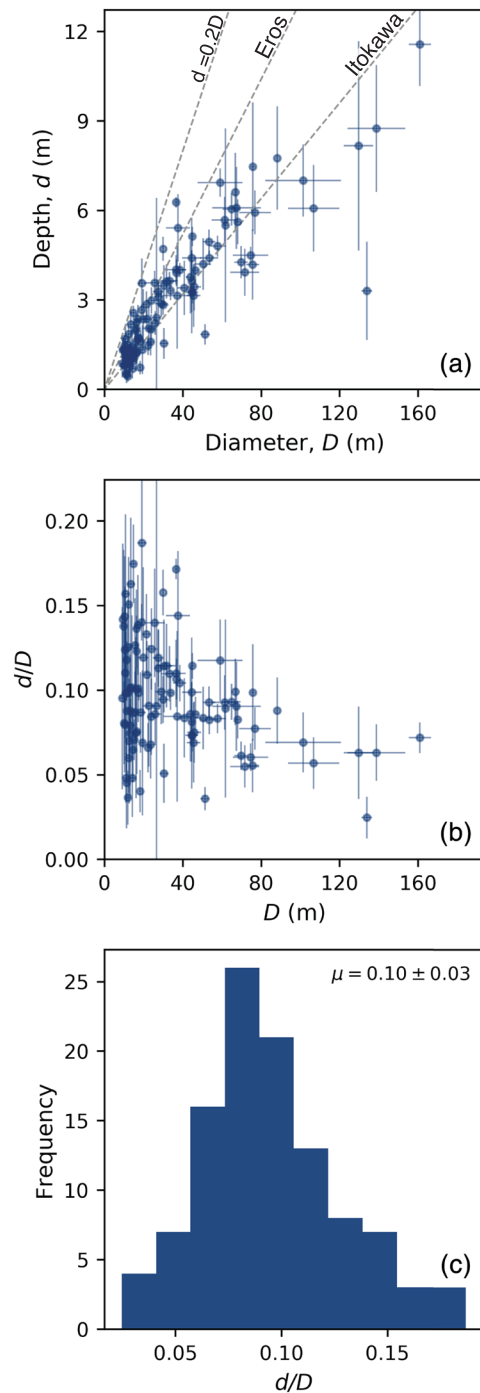
Figure 3. (a) The depths and diameters of 108 impact craters larger than 10 m on Bennu. Craters of similar sizes exhibit a broad range of depths. At diameters larger than ~80 m, the relationship between crater depth and diameter levels off, indicating that crater depth no longer necessarily increases with crater size. Dashed lines show the depth-diameter relationship for impact craters on Eros from Barnouin-Jha et al. (2001) and Itokawa from Hirata et al. (2009). (b) Plotting d/D as a function of crater diameter reveals that the smallest craters have the widest variation in d/D, the range of d/D narrows as crater size increases, and larger craters tend to have small d/D (i.e., be shallow). Section 2.2 describes how error bars were calculated. (c) The distribution of d/D is unimodal. The mean, μ, is 0.10. The standard deviation is 0.03. Histogram bins are 0.02 wide.

d/D have been correlated with surface units on Vesta (Vincent et al., 2014), Lutetia (Vincent et al., 2012), and the Moon (Stopar et al., 2017), for example. Owing to Bennu's rubble-pile character, target properties differ stochastically from place to place and depend on the packing, porosity, and orientations of blocks and boulders at each impact site. In this regime, changes in the geometry of the first contact between target and projectile, as well as the connectivity of target grains, can create a broad range of outcomes, including in crater depth, from similar initial impact conditions (Barnouin, Daly, Cintala, & Crawford, 2019; Tatsumi & Sugita, 2018). The scale of the impactor relative to particle sizes at the impact site (as well as impact velocity) also leads to variable d/D (Barnouin, Daly, Cintala, & Crawford, 2019). Hence, the rubble-pile nature of Bennu drives some of the variation in d/D on Bennu.

Direct evidence for the complexities posed by rubble-pile asteroids comes from the active impact experiment performed by the Hayabusa2 mission at asteroid Ryugu, an ~1-km-diameter C-type asteroid, using a copper projectile of ~2 kg with an impact speed of ~2 km s^{-1}. The crater that formed had a d/D of 0.15 ± 0.01 (Arakawa et al., 2020), although the reported depth included a "pit" formed near a large boulder. The presence of boulders near the impact site meaningfully affected crater formation and led to a crater with an irregular shape and interior. In addition, the crater diameter was larger than expected from strength scaling rules, suggesting that it was controlled solely by gravity on a surface with strength properties similar to that of cohesionless sand (Arakawa et al., 2020). The sizes and distribution of boulders can strongly affect crater morphology, even if they have only a modest effect on cratering efficiency. This result is consistent with experiments that investigate impacts in coarse-grained targets (Barnouin, Daly, Cintala, & Crawford, 2019).

4.4. Effects of Curvature on d/D of Large Craters

As noted in section 3 (see also Figure 3b), craters >80 m on Bennu have a narrower d/D range than the rest of the crater population, and their d/D values are small. These large craters are presumably some of the oldest on Bennu, which gives mass wasting and infilling processes a long time to operate. However, Walsh et al. (2019) and Jawin et al. (2020) found that the only large crater with signs of infilling, which they attributed to mass wasting, is the one shown in Figure 1f. Degradation and infilling thus are unlikely to be the sole causes of this narrow range.

Many of the large craters are planar with respect to the height in the direction normal to a best fit plane fit to all OLA points within the DTM. The crater rim, walls, and floor are essentially coplanar in this space. Profiles show that the centers of these large craters are frequently higher than the rims when plotted with respect to this height (Figure S6 shows two examples). Together, these observations are consistent with the removal of material from these locations, most likely by impact.

At these large scales, the curvature of Bennu becomes an important factor. Craters >80 m subtend a solid angle that covers a major fraction of Bennu. The region inside the largest crater (Figure 1f), for instance, accounts for ~3.5% of Bennu's total surface area. The small d/D of these large craters is consistent with past work assessing the effects of target curvature on impact cratering. Impact experiments reported by Fujiwara et al. (1993) into curved mortar cylinders or semispheres yielded a range of crater morphologies similar to those observed in large craters on Bennu,

including cases where the impact resulted in a very shallow crater with a muted rim or where the impact created a flat facet with no rim. In such cases, the impact feature was discerned via a preimpact and postimpact comparisons of the target shape (e.g., their Figure 3). Fujiwara et al. (1993) used strength-controlled targets, not a rubble pile on which some craters can be controlled by gravity, as found in the Hayabusa2 experiment. However, Asphaug et al. (1996) performed 3-D smoothed-particle hydrodynamic (SPH) impact simulations of impacts onto a shape model of the asteroid Ida and found that even in large, gravity-controlled craters, target curvature has an effect. In their simulations, the shape of the damaged region associated with the impact flattened as target curvature increased. The simulations did not run long enough to directly measure final crater shapes; however, the authors inferred that a flatter fracture cavity would lead to a flatter final crater.

We emulated the preimpact and postimpact comparisons of Fujiwara et al. (1993) by comparing the high-resolution, 20-cm GSD global OLA shape model (Daly et al., 2020) (i.e., postimpact Bennu) to a long-wavelength approximation of the global shape (i.e., preimpact Bennu). Preimpact Bennu was approximated by decomposing the high-resolution OLA model into spherical harmonics, and then reconstructing the global shape up to degree and order four. We then compared the two models at the location of each crater >100 m in diameter (e.g., Figure S7). If these large craters represent areas where material was ejected from the low-degree Bennu shape by an impact, then they should be depressed relative to the long-wavelength model, with the long-wavelength model doming above the crater floor. In nearly all cases, this is what we observe, which implies material was removed from the low-degree shape. Based on the morphologies seen in the Fujiwara et al. (1993) experiments, this finding supports an impact origin for these large features.

The properties of craters on Bennu can also indicate the presence and variation of strength within the asteroid. On Eros, target curvature effects become important only for the very largest craters, Himeros and Shoemaker, and these two craters are similar in scale to Eros itself (Robinson et al., 2002). The large, flat craters on Bennu are not quite so large relative to the body, which suggests that an additional factor must be at work. We posit that this factor is likely an increase in the strength of Bennu's materials with depth. An increase in strength with depth has been proposed on other asteroids such as Eros (Robinson et al., 2002). Despite being a rubble pile, Bennu shows evidence for internal stiffness, including terraces, rock channels, longitudinal ridges, and lineaments (Barnouin, Daly, Palmer, et al., 2019). Mound craters provide additional evidence for strength at depth (see section 4.5). The center-of-mass/center-of-figure offset measured by OSIRIS-REx could be explained by a few large boulders or shards in the interior of Bennu (Scheeres et al., 2019), and a large interior shard would likely be stronger than the surrounding gravitationally bound aggregate. A more competent layer at depth can lead to crater flattening as seen on the Moon, thereby decreasing d/D (Quaide & Oberbeck, 1968). The flattened morphologies of the largest craters on Bennu likely result from the combined effects of target curvature and the internal structure of Bennu, and target strength likely accentuates the effects of target curvature.

4.5. Inferences for Subsurface Structure From Mound Craters

Observations of impact craters on planetary surfaces (e.g., Bart, 2014; Bart et al., 2011; Quaide & Oberbeck, 1968), impact experiments (Quaide & Oberbeck, 1968), and numerical models (Senft & Stewart, 2007) indicate that central mounds form inside craters when the floor is located near the boundary between a weak upper layer and strong substrate (e.g., lunar regolith above bedrock). The literature does not report definitive examples of mound craters on other asteroids. Cheng et al. (2002) reported a suspected mound crater on Eros. Mound craters exist on Phobos (Basilevsky et al., 2014; Thomas, 1979). The presence of mound craters on Bennu is, therefore, somewhat unusual though not unprecedented.

The diameters of mound craters constrain the thickness of weak surface material and the depth to more competent material. Based on lunar examples and impact experiments, Quaide and Oberbeck (1968) showed that mound craters form when the ratio between the rim-to-rim diameter of the crater, D_r, and regolith thickness, t (i.e., thickness of weaker surface material) is between ~4 and ~7.5. Applying these results to Bennu implies that the three mound craters formed in places where a layer of weak material ~2 to 6 m deep (depending on the crater) lies atop a stronger, more competent substrate (Table S3).

The specific ranges of D_r/t that lead to mound craters on Bennu might differ from the values determined by Quaide and Oberbeck (1968) owing to differences in material properties (e.g., angle of repose) on Bennu

versus the Moon. However, numerical models indicate that the strength contrast between the two layers, rather than the absolute strengths of the upper material or substrate, is the relevant factor in mound crater formation (Senft & Stewart, 2007). In addition, Quaide and Oberbeck (1968) performed experiments on materials with a range of strength properties and observed mound crater formation in all cases, although the range of onset D_r/t varied modestly with material properties. Hence, the inference that mound craters on Bennu formed in a layer of weaker material atop a more competent substrate is robust. The absolute thickness of the weaker layer is not as well constrained due to the uncertainties in the material properties of Bennu's near and subsurface.

We hypothesize that these mound craters formed in regions underlain by a competent block or boulder. The literature (e.g., Bart, 2014; Bart et al., 2011; Quaide & Oberbeck, 1968; Senft & Stewart, 2007) is not sufficiently detailed to allow us to pinpoint the size of the stronger substrate relative to the size of the crater, but we speculate that the block would need to be wider than the crater itself. Only a few craters have central mounds, and they are geographically dispersed. The conditions that lead to mound formation, therefore, are not widespread. On the one hand, because Bennu is a rubble pile, one might expect craters to often form above a block or boulder, which would suggest that mound craters should be common. On the other hand, mound craters can form only when the layer of weaker material is a specific thickness relative to the size of the crater (Quaide & Oberbeck, 1968; Senft & Stewart, 2007), which would restrict the number of craters one would expect to contain mounds in a rubble pile. In addition, the subsurface block may need to be of a certain length scale with respect to the overlying crater or oriented subparallel to the preimpact surface, in which case the conditions for mound crater formation would be even less common.

5. Conclusions

We measured the diameters and depths of impact craters on Bennu larger than 10 m using data from the OSIRIS-REx Laser Altimeter. The average d/D is 0.10 ± 0.03 measured with respect to elevation, but d/D ranges from 0.02 to 0.19. The range of d/D likely reflects not only variations in crater degradation but also the effects of a coarse, rubble-rich target on crater formation. The range of d/D narrows as crater size increases, with craters >80 m tending toward smaller d/D. A few craters have central mounds, a trait that implicates the presence of competent material located a few meters beneath them. For craters >80 m, an increase in target strength with depth appears to affect crater morphometry, although target curvature likely also contributes. The results reported here highlight the role that impacts play in shaping the surfaces of rubble-pile asteroids and the how the physical properties of an asteroid can be inferred by studying its impact craters.

Conflict of Interest

The authors declare no real or perceived financial conflicts of interest.

Data Availability Statement

Data from OLA (Orbital B mission phase) and OCAMS (Approach, Preliminary Survey, and Detailed Survey mission phases) are publicly available in the Planetary Data System (PDS) (Daly et al., 2019; Rizk et al., 2019). Data are delivered to the PDS according to the timeline described in the OSIRIS Data Management Plan (Crombie & Selznick, 2019). The DTMs analyzed here are available in a permanent archive associated with this paper at http://lib.jhuapl.edu/papers/the-morphometry-of-impact-craters-on-bennu/ website.

References

Arakawa, M., Saiki, T., Wada, K., Ogawa, K., Kadono, T., Shirai, K., et al. (2020). An artificial impact on the asteroid (162173) Ryugu formed a crater in the gravity-dominated regime. *Science*, *368*(6486), 67–71. https://doi.org/10.1126/science.aaz1701

Asphaug, E., Moore, J. M., Morrison, D., Benz, W., Nolan, M. C., & Sullivan, R. J. (1996). Mechanical and geological effects of impact cratering on Ida. *Icarus*, *120*(1), 158–184. https://doi.org/10.1006/icar.1996.0043

Ballouz, R.-L., Walsh, K. J., Barnouin, O. S., DellaGiustina, D. N., Al Asad, M., Jawin, E. R., et al. (2020). Bennu's near-Earth lifetime of 1.75 million years inferred from craters on its boulders. *Nature*, *587*(7833), 205–209. https://doi.org/10.1038/s41586-020-2846-z

Barnouin, O. S., Daly, M. G., Palmer, E. E., Gaskell, R. W., Weirich, J. R., Johnson, C. L., et al. (2019). Shape of (101955) Bennu indicative of a rubble pile with internal stiffness. *Nature Geoscience*, *12*(4), 247–252. https://doi.org/10.1038/s41561-019-0330-x

Barnouin, O. S., Daly, M. G., Palmer, E. E., Johnson, C. L., Gaskell, R. W., al Asad, M., et al. (2020). Digital terrain mapping by the OSIRIS-REx mission. *Planetary and Space Science*, *180*, 104764. https://doi.org/10.1016/j.pss.2019.104764

Barnouin, O. S., Daly, R. T., Cintala, M. J., & Crawford, D. A. (2019). Impacts into coarse-grained spheres at moderate impact velocities: Implications for cratering on asteroids and planets. *Icarus*, *325*, 67–83. https://doi.org/10.1016/j.icarus.2019.02.004

Barnouin-Jha, O. S., Garvin, J. B., Cheng, A. F., Zuber, M., Smith, D., Neumann, G., et al. (2001). Preliminary impact crater dimensions on 433 Eros from the NEAR laser rangefinder and imager, abstract 1786. 32nd Lunar and Planetary Science Conference.

Bart, G. D. (2014). The quantitative relationship between small impact crater morphology and regolith depth. *Icarus*, *235*, 130–135. https://doi.org/10.1016/j.icarus.2014.03.020

Bart, G. D., Nickerson, R. D., Lawder, M. T., & Melosh, H. J. (2011). Global survey of lunar regolith depths from LROC images. *Icarus*, *215*(2), 485–490. https://doi.org/10.1016/j.icarus.2011.07.017

Basilevsky, A. T., Lorenz, C. A., Shingareva, T. V., Head, J. W., Ramsley, K. R., & Zubarev, A. E. (2014). The surface geology and geomorphology of Phobos. *Planetary and Space Science*, *102*, 95–118. https://doi.org/10.1016/j.pss.2014.04.013

Bierhaus, E., Barnouin, O., Walsh, K., Daly, T., Pajola, M., Jawin, E., et al. (2019). The appearance and size-frequency distribution of candidate impact craters on (101955) Bennu, EPSC-DPS2019-1134. EPSC-DPS joint meeting 2019.

Bierhaus, E. B., Barnouin, O., McCoy, T. J., Connolly, H. C., Jawin, E., Walsh, K. J., et al. (2019). Asteroid (101955) Bennu's crater population: Morphologies, size-frequency distribution, and consequences for surface age(s), abstract 2496. 50th Lunar and Planetary Science Conference.

Bierhaus, E. B., Trang, D., Barnouin, O. S., Daly, R. T., Walsh, K. J., Daly, M. G., et al. (2020). Detailed characterization of crater types and relationships to surface and sub-surface structure on Bennu, abstract 2156. 51st Lunar and Planetary Science Conference.

Carr, M. H., Kirk, R. L., McEwen, A., Veverka, J., Thomas, P., Head, J. W., & Murchie, S. (1994). The geology of Gaspra. *Icarus*, *107*(1), 61–71. https://doi.org/10.1006/icar.1994.1006

Cheng, A. F., Barnouin-Jha, O., Prockter, L., Zuber, M. T., Neumann, G., Smith, D. E., et al. (2002). Small-scale topography of 433 Eros from laser altimetry and imaging. *Icarus*, *155*(1), 51–74. https://doi.org/10.1006/icar.2001.6750

Crombie, M. K., & Selznick, S. (2019). Origins, Spectral Interpretation, Resource Identification, Security, Regolith Explorer (OSIRIS-REx): Mission bundle. NASA Planetary Data System, urn: nasa: pds: orex. mission. https://sbn.psi.edu/pds/resource/orex/orexmission.html

Daly, M., Barnouin, O., Espiritu, R., & Lauretta, D. (2019). Origins, Spectral Interpretation, Resource Identification, Security, Regolith Explorer (OSIRIS-REx): OSIRIS-REx Laser Altimeter Bundle, urn:nasa:pds:orex.ola, NASA Planetary Data System.

Daly, M. G., Barnouin, O. S., Dickinson, C., Seabrook, J., Johnson, C. L., Cunningham, G., et al. (2017). The OSIRIS-REx Laser Altimeter (OLA) investigation and instrument. *Space Science Reviews*, *212*(1–2), 899–924. https://doi.org/10.1007/s11214-017-0375-3

Daly, M. G., Barnouin, O. S., Seabrook, J. A., Roberts, J., Dickinson, C., Walsh, K. J., et al. (2020). Hemispherical differences in the shape and topography of asteroid (101955) Bennu. *Science Advances*, *6*(41), eabd3649. https://doi.org/10.1126/sciadv.abd3649

DellaGiustina, D. N., Emery, J. P., Golish, D. R., Rozitis, B., Bennett, C. A., Burke, K. N., et al. (2019). Properties of rubble-pile asteroid (101955) Bennu from OSIRIS-REx imaging and thermal analysis. *Nature Astronomy*, *3*(4), 341–351. https://doi.org/10.1038/s41550-019-0731-1

Fujiwara, A., Kadono, T., & Nakamura, A. (1993). Cratering experiments into curved surfaces and their implication for craters on small satellites. *Icarus*, *105*(2), 345–350. https://doi.org/10.1006/icar.1993.1131

Golish, D. R., Drouet d'Aubigny, C., Rizk, B., DellaGiustina, D. N., Smith, P. H., Becker, K., et al. (2020). Ground and in-flight calibration of the OSIRIS-REx camera suite. *Space Science Reviews*, *216*(1), 12. https://doi.org/10.1007/s11214-019-0626-6

Hamilton, V. E., Simon, A. A., Christensen, P. R., Reuter, D. C., Clark, B. E., Barucci, M. A., et al. (2019). Evidence for widespread hydrated minerals on asteroid (101955) Bennu. *Nature Astronomy*, *3*(4), 332–340. https://doi.org/10.1038/s41550-019-0722-2

Hergenrother, C. W., Nolan, M. C., Binzel, R. P., Cloutis, E. A., Barucci, M. A., Michel, P., et al. (2013). Lightcurve, color and phase function photometry of the OSIRIS-REx target asteroid (101955) Bennu. *Icarus*, *226*(1), 663–670. https://doi.org/10.1016/j.icarus.2013.05.044

Hirata, N., Barnouin-Jha, O. S., Honda, C., Nakamura, R., Miyamoto, H., Sasaki, S., et al. (2009). A survey of possible impact structures on 25143 Itokawa. *Icarus*, *200*(2), 486–502. https://doi.org/10.1016/j.icarus.2008.10.027

Jawin, E. R., Walsh, K. J., Barnouin, O. S., McCoy, T. J., Ballouz, R.-L., DellaGiustina, D. N., et al. (2020). Global patterns of recent mass movement on asteroid (101955) Bennu. *Journal of Geophysical Research: Planets*, *12*, e2020JE006475. https://doi.org/10.1029/2020je006475

Lauretta, D. S., Balram-Knutson, S. S., Beshore, E., Boynton, W. V., Drouet d'Aubigny, C., DellaGiustina, D. N., et al. (2017). OSIRIS-REx: Sample return from asteroid (101955) Bennu. *Space Science Reviews*, *212*(1–2), 925–984. https://doi.org/10.1007/s11214-017-0405-1

Lauretta, D. S., Bartels, A. E., Barucci, M. A., Bierhaus, E. B., Binzel, R. P., Bottke, W. F., et al. (2015). The OSIRIS-REx target asteroid (101955) Bennu: Constraints on its physical, geological, and dynamical nature from astronomical observations. *Meteoritics & Planetary Science*, *50*(4), 834–849. https://doi.org/10.1111/maps.12353

Lauretta, D. S., DellaGiustina, D. N., Bennett, C. A., Golish, D. R., Becker, K. J., Balram-Knutson, S. S., et al. (2019). The unexpected surface of asteroid (101955) Bennu. *Nature*, *568*(7750), 55–60. https://doi.org/10.1038/s41586-019-1033-6

Marchi, S., Chapman, C. R., Barnouin, O. S., Richardson, J. E., & Vincent, J.-B. (2015). Cratering on asteroids. In P. Michel, F. E. DeMeo, W. F. Bottke (Eds.), *Asteroids IV* (pp. 725–744). Tucson, AZ, USA: University of Arizona Press.

Noguchi, R., Hirata, N., Hirata, N., Shimaki, Y., Nishikawa, N., Tanaka, S., et al. (2021). Crater depth-to-diameter ratios on asteroid 162173 Ryugu. *Icarus*, *354*, 114016. https://doi.org/10.1016/j.icarus.2020.114016

Quaide, W. L., & Oberbeck, V. R. (1968). Thickness determinations of the lunar surface layer from lunar impact craters. *Journal of Geophysical Research*, *73*(16), 5247–5270. https://doi.org/10.1029/JB073i016p05247

Rizk, B., Drouet d'Aubigny, C., Golish, D., Fellows, C., Merrill, C., Smith, P., et al. (2018). OCAMS: The OSIRIS-REx camera suite. *Space Science Reviews*, *214*(1), 26. https://doi.org/10.1007/s11214-017-0460-7

Rizk, B., Drouet d'Aubigny, C., Golish, D., DellaGiustina, D. N., & Lauretta, D. S. (2019). Origins, Spectral Interpretation, Resource Identification, Security, Regolith Explorer (OSIRIS-REx): OSIRIS-REx Camera Suite (OCAMS) bundle, urn:nasa:pds:orex.ocams, NASA planetary data system.

Robinson, M. S., Thomas, P. C., Veverka, J., Murchie, S. L., & Wilcox, B. B. (2002). The geology of 433 Eros. *Meteoritics & Planetary Science*, *37*(12), 1651–1684.

Robbins, S. J., Watters, W. A., Chappelow, J. E., Bray, V. J., Daubar, I. J., Craddock, R. A., et al. (2018). Measuring impact crater depth throughout the solar system. *Meteoritics & Planetary Science*, *53*(4), 583–637. https://doi.org/10.1111/maps.12956

Scheeres, D. J., McMahon, J. W., French, A. S., Brack, D. N., Chesley, S. R., Farnocchia, D., et al. (2019). The dynamic geophysical environment of (101955) Bennu based on OSIRIS-REx measurements. *Nature Astronomy*, *3*(4), 352–361. https://doi.org/10.1038/s41550-019-0721-3

Schultz, P. H. (1988). Cratering on mercury—A relook. In F. Vilas, C. R. Chapman, M. S. Matthews (Eds.), *Mercury* (pp. 274–335). Tucson, AZ, USA: University of Arizona Press.

Senft, L. E., & Stewart, S. T. (2007). Modeling impact cratering in layered surfaces. *Journal of Geophysical Research*, *112*, E11002. https://doi.org/10.1029/2007JE002894

Stopar, J. D., Robinson, M. S., Barnouin, O. S., McEwen, A. S., Speyerer, E. J., Henriksen, M. R., & Sutton, S. S. (2017). Relative depths of simple craters and the nature of the lunar regolith. *Icarus*, *298*, 34–48. https://doi.org/10.1016/j.icarus.2017.05.022

Sugita, S., Honda, R., Morota, T., Kameda, S., Sawada, H., Tatsumi, E., et al. (2019). The geomorphology, color, and thermal properties of Ryugu: Implications for parent-body processes. *Science*, *364*, eaaw0422. https://doi.org/10.1126/science.aaw0422

Sullivan, R., Greeley, R., Pappalardo, R., Asphaug, E., Moore, J. M., Morrison, D., et al. (1996). Geology of 243 Ida. *Icarus*, *120*(1), 119–139. https://doi.org/10.1006/icar.1996.0041

Tatsumi, E., & Sugita, S. (2018). Cratering efficiency on coarse-grain targets: Implications for the dynamical evolution of asteroid 25143 Itokawa. *Icarus*, *300*, 227–248.

Thomas, P. (1979). Surface features of Phobos and Deimos. *Icarus*, *40*(2), 223–243. https://doi.org/10.1016/0019-1035(79)90069-1

Thomas, P. C., Veverka, J., Bell, J. F., Clark, B. E., Carcich, B., Joseph, J., et al. (1999). Mathilde: Size, shape, and geology. *Icarus*, *140*(1), 17–27. https://doi.org/10.1006/icar.1999.6121

Veverka, J. (1997). NEAR's flyby of 253 Mathilde: Images of a C asteroid. *Science*, *278*(5346), 2109–2114. https://doi.org/10.1126/science.278.5346.2109

Vincent, J.-B., Besse, S., Marchi, S., Sierks, H., & Massironi, M. (2012). Physical properties of craters on asteroid (21) Lutetia. *Planetary and Space Science*, *66*(1), 79–86. https://doi.org/10.1016/j.pss.2011.12.025

Vincent, J. -B., Schenk, P., Nathues, A., Sierks, H., Hoffmann, M., Gaskell, R. W., et al. (2014). Crater depth-to-diameter distribution and surface properties of (4) Vesta. *Planetary and Space Science*, *103*(Supplement C), 57–65. https://doi.org/10.1016/j.pss.2013.09.003

Walsh, K. J., Jawin, E. R., Ballouz, R.-L., Barnouin, O. S., Bierhaus, E. B., Connolly, H. C., et al. (2019). Craters, boulders and regolith of (101955) Bennu indicative of an old and dynamic surface. *Nature Geoscience*, *12*(4), 242–246. https://doi.org/10.1038/s41561-019-0326-6

Watanabe, S., Hirabayashi, M., Hirata, N., Hirata, N., Noguchi, R., Shimaki, Y., et al. (2019). Hayabusa2 arrives at the carbonaceous asteroid 162173 Ryugu—A spinning top–shaped rubble pile. *Science*, *364*(6437), 268–272. https://doi.org/10.1126/science.aav8032

References From the Supporting Information

Seabrook, J. A., Daly, M. G., Barnouin, O. S., Johnson, C. L., Nair, A. H., Bierhaus, E. B., et al. (2019). Global shape modeling using the OSIRIS-REx scanning Laser Altimeter. *Planetary and Space Science*, *177*, 104688. https://doi.org/10.1016/j.pss.2019.07.003

Werner, R. A., & Scheeres, D. J. (1997). Exterior gravitation of a polyhedron derived and compared with harmonic and mascon gravitation representations of asteroid 4769 Castalia. *Celestial Mechanics and Dynamical Astronomy*, *65*, 313–344.